Soft Matter

Conformationally Directed Assembly of Peptides on 2D Solid Surfaces Mediated by Thermal Stimuli

Journal:	*Soft Matter*
Manuscript ID	SM-ART-02-2019-000426.R1
Article Type:	Paper
Date Submitted by the Author:	10-Jul-2019
Complete List of Authors:	Jorgenson, Tyler; University of Washington, Molecular Engineering and Sciences Institute Milligan, Madelyn; University of Washington, Material Science and Engineering Sarikaya, Mehmet; University of Washington, Material Science and Engineering Overney, Rene; University of Washington, Chemical Engineering

Conformationally Directed Assembly of Peptides on 2D Surfaces Mediated by Thermal Stimuli

Tyler D. Jorgenson,[a] Madelyn Milligan,[b] Mehmet Sarikaya,[a,b] and René M. Overney*[a,c]

Dynamic and environmentally directed assembly of molecules in biological systems is essential for the fabrication of microscale, hierarchical, functional structures. Here, we demonstrate the directed assembly of genetically selected graphite binding peptides on 2D solid surfaces upon thermal stimulus. Structural and kinetic analyses as well as molecular dynamics simulations yield the self-assembly process as thermally controllable upon tuning the solvated peptide conformational state. The ability to tailor the structure of two-dimensional soft bio/nano interfaces *via* external stimuli would allow for the bottom-up fabrication of complex materials with nanotechnological importance, such as biosensors, bioelectronics, and biomolecular fuel cells.

Introduction

Molecular self-assembly involves spontaneous structuring or self-organization of molecules in solution and at interfaces. It is a ubiquitous phenomenon observed at multiple length scales and is a key strategy in building biological architectures and molecular machines that execute life's functions.[2-5] Inspired by nature, a wide variety of methods have been developed to aid nanoscale organization of molecules and nanomaterials in solution and at free surfaces enabling bottom-up fabrication in both nano- and bio-technologies.[6-8] Molecular assembly relies on relatively weak forces, such as van der Waals (VdW), hydrogen bonding, and electrostatic interactions.[9, 10]

Self-assembling systems can be grouped concerning their monomeric structure rigidity, and, whether the intermolecular interactions are orientationally sensitive. Inorganic particles and many synthetic small molecules possess more static/rigid structures yielding self-assemblies that rely predominantly on van der Waals interactions, *e.g.,* lipid micelle formations in solution, or alkane-thiol assembly at surfaces.[8, 11-13] Synthetic organic molecules that have been engineered to assemble through orientationally sensitive interactions, such as hydrogen bonding or π-π interactions, allow for directional control over the assembly structure.[10, 14] Orientationally sensitive interactions are structurally unforgiving, so that rigid monomers must be perfectly shaped to obtain proper assembly. Due to the foremost "rigid" structure of the monomer, the self-assembly process is accurately described by relatively simple thermodynamic and kinetic models.[15]

In biomolecular systems, monomer structural differences profoundly affect self-assembly due to the orientational dependence of intermolecular interactions, and, the increased conformational degrees of freedom of the molecule. This conformational dependence of the self-assembly process typically necessitates interactions between monomers with well-defined biomolecular structures and chemistries, *e.g.* "lock-and-key" associations, as found for ligand-receptor or antibody-antigen interactions.[16, 17] Biomolecules either possess well-defined structures, or adopt them upon interacting with their binding partners, described by the "induced fit model".[16] Due to the complexity and specificity of biomolecular interactions, biomolecules have garnered interest as a means of engineering complex hierarchically assemblies of technological importance.[18-24] Traditional kinetic models typically apply to the assembly of thermally stable biomolecules, such as micelle formation, fibrillation, *etc.*, enabling their use in engineering applications.[20, 25, 26]

Conformational dependences of biomolecular interactions can be utilized to dynamically control assembly by inducing an "active" conformational state, *e.g.* cytoskeleton filament assembly.[5, 27, 28] Well-defined structures are not *a priori* required for assembly, as long as there exists a conformational state that leads to assembly. Intrinsically disordered proteins, a class of biomolecules ranging from completely unstructured to dynamically structured conformations, highlight the phenomenon of self-assembly with metastable conformational states with increased intermolecular interactions.[29-32]

Peptides genetically selected to bind to metal, ceramic and mineral surfaces are commonly viewed as part of this class of intrinsically disordered biomolecules.[33-35] Despite the assumed structural disorder of solid binding peptides (SBPs), some exhibit long range ordered assembly on solids for which they were selected.[36, 37] The material-specificity and self-assembling capability of SBPs are core in their use as molecular linkers, assemblers, and inorganic synthesizers for bio-enabled

a. Molecular Engineering and Sciences Institute, University of Washington, Seattle, WA
b. Department of Material Science and Engineering, University of Washington, Seattle, WA
c. Department of Chemical Engineering, University of Washington, Seattle, WA

technologies.[38-42] The assembly process of SBPs has been shown to depend on the adsorption kinetics and strength, surface diffusion, and intermolecular interactions between peptides.[36] For example, two chemically similar graphite binding peptides that differ in the composition of the C-terminal aromatic residues (GrBP5-WT and GrBP5-M2), detailed in Fig. 1, assemble into two different structures on graphite.[36] It was shown that GrBP5-WT (WT) form long-range ordered nanostrips up to microns in length with six-fold symmetry, mirroring the underlying graphite lattice. Experimental and computational work on GrBP5-WT self-assembly suggested the long-range ordering requires non-bonding weak intermolecular interactions including hydrogen bonding and hydrophobic van der Waals.[36, 43] GrBP5-M2 (M2), on the other hand, form confluent amorphous films. The difference in assembly was attributed to increased aromaticity of M2 leading to tighter binding and slower surface diffusion.[36]

Peptide	MW	Charge	pI	GRAVY
GrBP5-WT	1383.4	-2	3.55	-.242
GrBP5-M2	1427.5	-2	3.55	-.175

Fig. 1 Sequence and physical properties of GrBP5-WT and GrBP5-M2. The displayed charge is the net charge of the peptide at pH 7, in which the N and C terminus as well as the central E and D are charged. The molecular weight (MW) is in Daltons. The isoelectric point, pI, was determined using the IPC – Isoelectric Point Calculator.[1] The Grand Average Hydropathy (GRAVY) scores were determined as the sum of the individual amino acid hydropathies divided by the length of the peptide. The color coding for the amino acids is as follows: green – hydrophobic, yellow – sulfur containing, red – charged, orange – hydrophilic, blue – aromatic.

Since the observed SBP assemblies exhibit low-dimensionality and high coordination, it is reasonable to assume the assembly process/structures rely on orientationally and structurally sensitive interactions, as discussed above. Thus, it is necessary to complement the underlying adsorption and assembly parameters of SBPs with information about the conformational state (or states) of the peptides in solution. For instance, sequence differences between WT and M2 could result in different conformational or structural states in solution, and exhibit disparate responses to environmental conditions, such as temperature. In this light, the "rigid" monomer structure description of molecules must be replaced by a "soft" conformable depiction of the peptide structure in solution. This dynamic interpretation of structure suggests that solution conformational states could be biased to favor a particular self-assembly via changes in the solution environmental condition, e.g., incubation temperature. To predict and direct the assembly of SBPs, an understanding of how sequence and environmental conditions affect the peptide structure and the assembly must be developed. To this end, we investigate here (i) the energetic and structural effects of temperature on self-assembly with thermal and kinetic property experiments, in addition to (ii) molecular mechanics simulations of the solution dispersity of peptide conformations.

Experimental

Peptide Synthesis

The GrBP5-WT and GrBP5-M2 were synthesized in-house using an automated solid-phase peptide synthesizer (C2336X, CSBio Inc., Menlo Park, CA) employing standard batch process Fmoc (Fluorenylmethyloxycarbonyl) chemistry procedures as reported previously.[37] Fmoc deprotection was achieved using 20% piperidine in dimethyl formamide (DMF) and the reaction efficiency was monitored by UV absorbance at 301 nm. The peptides were cleaved from the resin and side chains were deprotected via mixing in a cleavage "cocktail" for 2 hours under a N_2 atmosphere. The cleavage cocktail contained trifluoroacetic acid (TFA) / thianisole / diH2O / phenol / ethanedithiol (EDT) (87.5:5:5:2.5) or TFA / tri-isopropylsilane / diH2O / EDT (94:1:2.5:2.5) for GrBP5-WT and GrBP5-M2 respectively. The peptide was separated from the resin, subsequently precipitated with cold ether, and reconstituted using various ratios of deionized water and acetonitrile. Purification by HPLC (Waters Deltaprep 600, Semi-preparation Mode) was performed using a linear gradient of 1% per minute at a flow rate of 10 mL/min. Retention times were anywhere between 30 and 50 minutes. The synthesized peptide's molecular weight was confirmed by MALDI-TOF mass spectrometry (Autoflex II, Bruker Daltonics, Billerica, MA). Spectra are provided in the supplementary materials.

Isothermal Peptide Assembly

Highly-oriented pyrolytic graphite (HOPG, Grade 1, SPI Inc.) was mechanically cleaved with scotch tape and attached via double sided tape to steel pucks. For peptide assembly, 40 μL of either 500 nM, 1 μM, 2.5 μM, or 5 μM peptide in deionized water was incubated for 3 hours on a freshly cleaved HOPG surface in a chamber with saturated water vapor at temperatures from 5°C to 47°C. After the incubation time elapsed the peptide solution was wicked from the surface using a laboratory tissue paper and subsequently dried under a gentle nitrogen flow for at least 30 seconds.

Non-Isothermal Peptide Assembly

To test for the effects of temperature on the solvated peptide, 200 μL of 2.5 μM peptide was heated to an elevated

ARTICLE

temperature (37°C for WT and 47°C for M2). After 15, 30, and 60 minutes of exposure to heat, 40 µL of the heated peptide solution was quenched to room-temperature and incubated on a freshly cleaved HOPG surface (see substrate preparation above) in a chamber with saturated water vapor for 3 hours. To test the effect of temperature on the peptide surface dynamics, 40 µL of peptide solution was incubated at room temperature on HOPG surfaces for 1 hour, at which point the sample was exposed to an elevated temperature for an additional 3 to 6 hours. The samples were dried using the same procedure as isothermal experiments.

AFM Imaging and Image Analysis

Dried self-assembled peptide samples were kept in a dry environment until imaged by atomic force microscopy (AFM Nanoscope IIIa, Digital Instruments) in tapping mode under ambient conditions using soft tapping mode AFM probes (HQ:NSC14/No Al, MikroMasch). AFM images were analysed using Gwyddion 2.52 analysis software (gwyddion.net). Images were flattened and corrected for line errors. Total surface coverage was determined by masking the AFM images based on a threshold height that distinguished the peptides from the HOPG surface. The percent of ordering was deduced from the fraction of the total surface coverage that is part of a long range assembled structure. These regions were determined by thresholding the initial mask based on either the area or aspect ratio of individual grains. For samples of densely packed peptide, manual editing of the mask was used to distinguish between ordered and amorphous regions. Example masking and analysis is available in the supplementary material. At least three 1 µm² areas were analysed for each sample. Averages and standard deviations were determined from all individual image measurements.

Molecular Dynamics Set-up and Analysis

Simulations were performed using the *in lucem Molecular Mechanics* (ilmm) package with the microcanonical NVE (constant number of particles, volume, and energy) thermodynamic ensemble, and the flexible three-center (F3C) water model.[44-46] All simulations were performed at 298 K, pH 7, with no additional salt. The simulation temperature defines the Boltzmann distribution from which initial velocities are sampled. No thermostat regulates this distribution during the simulation; thus, velocity fluctuations were monitored to ensure neither temperature nor energy diverge. Protein Data Bank (PDB) files were built using *UCSF Chimera* (www.cgl.ucsf.edu).[47] Hydrogen atoms were modeled onto the protein structure and minimized for 500 steps of steepest gradient minimization. Afterwards the entire system is minimized for an additional 1000 steps. Water molecules were subsequently added, minimized for 100 steps, simulated for 500 steps, and minimized for an additional 500 steps. The peptide was then minimized in the presence of the water for 500 steps. An unbiased extended starting structure (Φ, Ψ = 180°) was simulated for 5-ns to generate a slightly collapsed structure to

be used for the subsequent 200-ns simulation. An 8 Å buffer region of water was used to prevent edge effects.

(Φ, Ψ) pairs were binned into a 2D histogram with 72 × 72 bins comprising 5° × 5° increments. The bins were scaled by the total number of (Φ, Ψ) pairs generating a population distribution for the backbone angles. These backbone angle distributions were used to calculate entropy values using $S = -R\sum A(i,j) \ln[A(i,j)]$, in which A is a population distribution and A(i,j) is the population density in one 5° × 5° bin. Free energy values for conformational states were determined using $G = -RT \times \ln[p_i/(1-p_i)]$, in which p_i is the probability of the conformational state based on the relative frequency of the state versus all observed states. The frequency and number of conformational states was obtained by ensemble clustering implemented in *UCSF Chimera*.

Results and discussion

Kinetic and Structural Analysis

To test the thermal effects and to probe the energetic landscape of WT and M2, we analyzed experimentally the equilibrium structures resulting from a variety of isothermal incubations. Atomic force microscopy (AFM) images displayed in Fig. 2a reveal for WT comparable equilibrium surface coverages at 23°C and 5 °C. At these incubation temperatures, the degree of ordering is above 60% for all samples with solution concentrations greater than 1 µM. Estimation of the equilibrium kinetics from Langmuir fits, Fig. 2b, show that adsorption kinetics and equilibrium surface coverages of WT decrease when the incubation temperature is increased beyond 23 °C. Similarly, the degree of ordering decreases with increased incubation temperature, Fig. 2c. Samples incubated at 37 °C had a maximum surface coverage of ~40 % and exhibited no ordering, even at high solution concentration of 5 µM.

In contrast to WT, the maximum surface coverage for M2 remains high (80 to 90%) for concentrations of 2.5 and 5 µM up to 47°C incubation temperatures, as revealed by AFM images and Langmuir isotherms in Figs. 3a and 3b, respectively. The equilibrium surface coverage at lower concentrations is more variable and affected by the incubation temperature. The degree of ordering in M2 samples, Fig. 3c, increases with elevated incubation temperature reaching above 80 % for 5 µM samples incubated at 47°C. Although increasing temperature aids M2 assembly, the results are inconsistent and do not follow an obvious trend with temperature. For example, more ordering was observed at 27 °C than at higher temperatures for 1 µM samples. Only the 2.5 µM samples followed the expected trend of increasing ordering with increasing temperature. The lack of observed ordering for 5 µM samples may be attributed to the high packing density in these samples. High packing density provides two challenges: (i) Restricted surface diffusion, and, thus annealing towards ordered assembly structures, as well as, (ii) Experimental difficulties in distinguishing the ordered from amorphous regions.
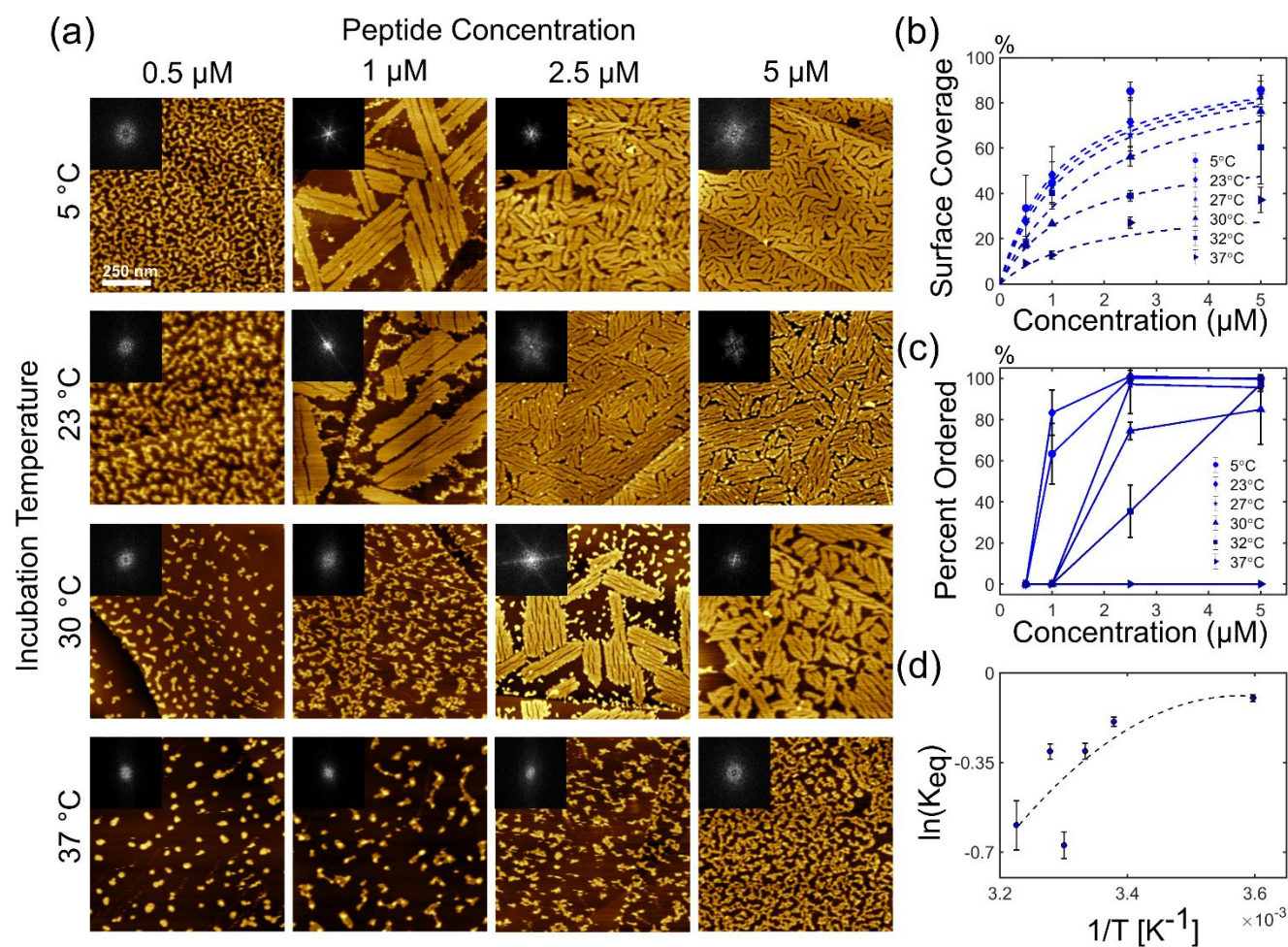
Fig. 2 WT Isothermal Assembly (a) Representative images of GrBP5-WT assembled structure for a variety of incubation temperatures and peptide concentrations. All images are 1 μm² and insets are Fast Fourier Transforms (FFTs) of the image. (b) Langmuir isotherms of equilibrium surface coverage. Dashed lines are fits from the Langmuir adsorption isotherm. (c) Percent ordering observed for each incubation condition tested. (d) Arrhenius plot of estimated equilibrium adsorption kinetic rates versus temperature showing non-linear relationship. The dashed line highlights the non-linearity of the Arrhenius plot.

The equilibrium adsorption kinetics for both WT and M2 are non-Arrhenius, *i.e.*, not loglinear with inverse temperature, as shown in Figs. 2d and 3d. Non-Arrhenius adsorption, with temperature dependent activation energies, suggest the structural dispersity of the peptide in solution changes, given the adsorption of biomolecules has been shown to depend on the solvated conformation.[48, 49] We observed aggregation (bright globular structures in Fig. 2a and Fig. 3a) at high temperature and low concentration for both WT and M2 samples, reducing the accuracy of the Langmuir fits for adsorption kinetics.

For WT, the non-Arrhenius behavior, highlighted by the curved guiding line in Fig. 2d, can be interpreted as denaturation, or, increased dispersity of the solvated structures. Increasing the incubation temperature results in reduced adsorption and subsequent loss in degree of ordering. In contrast to WT, non-Arrhenius behavior observed for M2 is discontinuous, with two regimes separated by a transition at a critical temperature around 30 °C (Fig. 3d). Above this critical temperature, ordering in M2 samples increases, especially for 2.5 μM samples (Fig. 3c). We attribute this transition to a change in the structural dispersity towards a conformation with a higher propensity of ordering at the surface.

Deconvoluting Solution and Surface Dynamics

The non-Arrhenius adsorption kinetics for WT and M2, Fig. 2d and 3d, suggest a temperature dependent chemical potential difference, Δμ(T), between the solvated peptide's self-energy and the self-energy of the adsorbed states. To investigate our hypothesis that changes in Δμ are a result of thermally induced conformational changes of the solvated peptides, we conducted non-isothermal assembly experiments (Fig. 4a). Briefly, 2.5 μM peptide solutions were exposed to an elevated temperature prior to introducing them at room temperature to HOPG surfaces for 3 hours. A 2.5 μM solution concentration was chosen for its clear change in assembly properties for both WT and M2 in isothermal experiments.

As shown in Fig. 4b, increasing the exposure time of the peptide solution to elevated temperatures, improved the degree of ordering for M2, while slightly impeding the ordering of WT. The surface coverage of WT samples decreased from 87% to 45% upon exposure to 1 hour of elevated temperature, corroborating the change in adsorption kinetics observed in isothermal experiments to be in part due to thermal effects on the solvated peptide conformation. The lack of ordering in isothermal experiments of WT can be interpreted to originate from an increase in the desorption rate at elevated
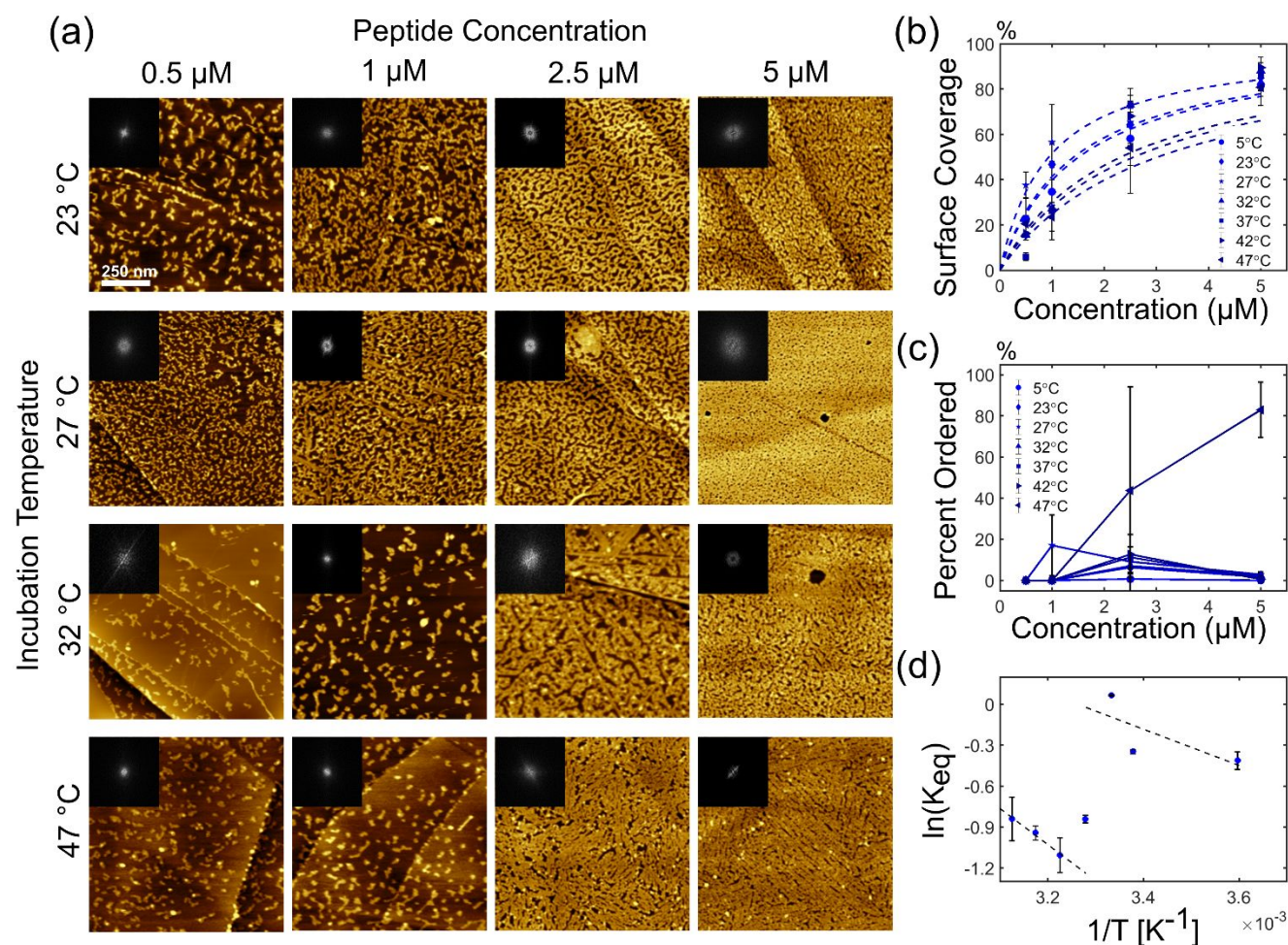
Fig. 3 Isothermal M2 Assembly. (a) Representative images of GrBP5-M2 assembled structure for a variety of incubation temperature and peptide concentrations. All images are 1 μm²and insets are Fast Fourier Transforms (FFTs) of the image. (b) Langmuir isotherms of equilibrium surface coverage. Dashed lines are fits from the Langmuir adsorption isotherm. (c) Percent ordering observed for each incubation condition tested. (d) Arrhenius plot of estimated equilibrium adsorption kinetic rates versus temperature showing non-linear relationship. Two linear fits are displayed to show discontinuity.

temperatures, affecting the aggregation and assembly. The surface coverage of pre-heated M2 remained high for all exposure times, as expected from isothermal experiments. These results corroborate the hypothesis that thermal energy affects the peptide in solution, and consequently leads to a different self-assembled structure.

Although preheating M2 in solution biased the peptide towards assembly, the extent of ordering is lower than observed for isothermal assembly. Peptide self-assembly on solid-surfaces is a multistep process involving the solution state, adsorption, diffusion and peptide-peptide interactions; all of which can be thermally modulated. To further interrogate the effects of temperature on the surface dynamics of the peptide, a second set of non-isothermal experiments were performed, Fig. 4(c-d), in which room-temperature peptide solutions were incubated on a fresh HOPG surface for 1 hour before "annealing" the incubated sample at an elevated temperature for three hours. The assembly structure of WT from a room-temperature peptide solution showed to be unaffected, *i.e.,* thermally stable after annealing for 6 hours at 37 °C, Fig. 4d(top). The M2 assembly, on the other hand, showed an increase in ordering at a rate of approximately 10% every 3

hours, Fig. 4d(bottom), implying the assembly process to be thermally activated on the surface, albeit a slower kinetic rate.

Combining the isothermal and non-isothermal experimental results, it can be concluded that peptide self-assembly is dependent on the solvated conformation. In the case of WT, peptides can be primed conformationally for assembly at room-temperature and colder incubations. Increasing the thermal energy of the peptide solution denatures the solute conformation leading to lower adsorption coverage and rate, thus, impeding ordering, as demonstrated in Fig. 2a,d and Fig. 4b. For M2, the transition to a conformation with higher propensity of ordering is similarly controlled via the temperature and can occur either in solution or at the surface. However, as demonstrated by the isothermal experiments, the combination of thermal exposure through-out the assembly process greatly enhances the adsorption kinetics, as well as, the degree of ordering.

Simulated Structural Propensities and Energetics

The experimental results highlight the role of solvated GrBP5 conformations in the peptide assembly kinetics and structure. To further elucidate the structural and energetic differences between WT and M2 in solution, we modelled their
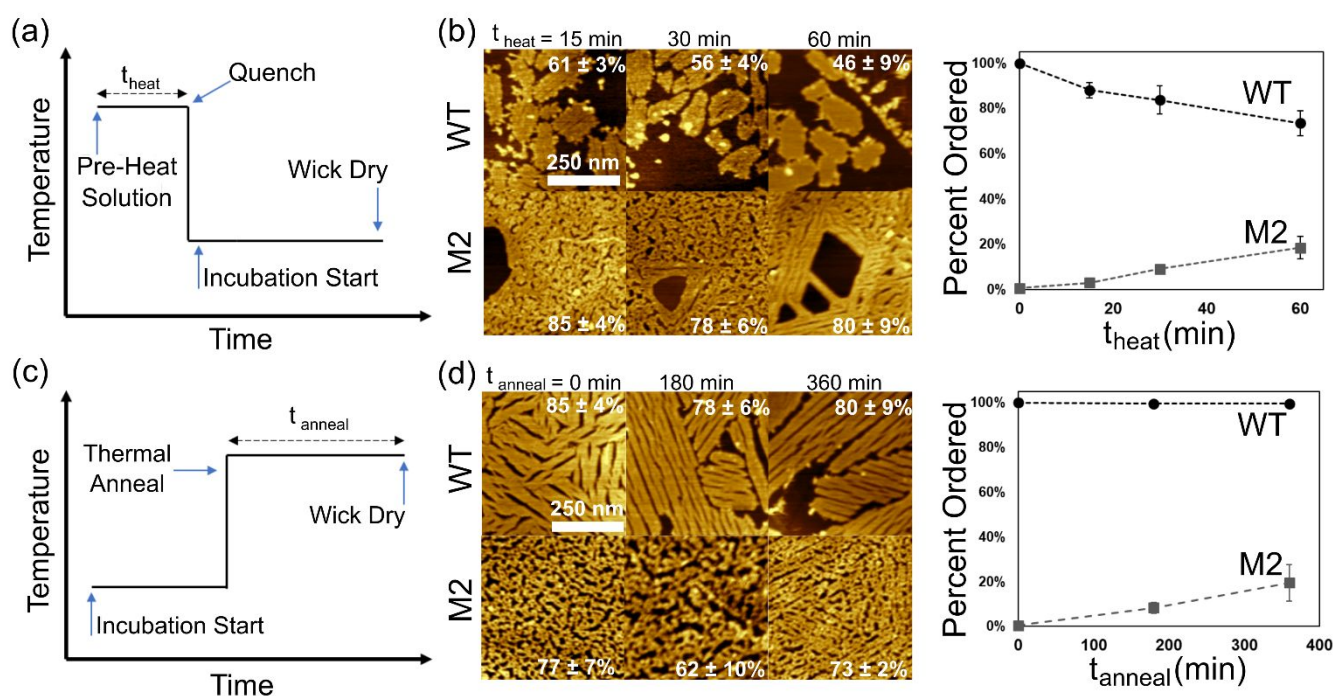
Fig. 4 Non-isothermal Assembly. (a) Schematic of the non-isothermal procedure used to obtain the data presented in (b). (b) Representative images of the self-assembled structures of WT and M2 as a function of exposure time to elevated pre-incubation temperatures. Quantification of the degree of ordering present in the self-assembled structures is displayed to the left. (c) Schematic of the non-isothermal procedure used to obtain data presented in (d). (d) Representative images of the self-assembled structures obtained from pre-incubating the peptide and thermal annealing for different durations (right) and the quantification of the degree of ordering (left). A temperature of 37°C was used for WT samples while M2 was exposed to 47°C. Inset percentages on AFM images are the total surface coverage of the samples.

conformational propensities using *in lucem Molecular Mechanics* (*ilmm*).[45] To identify stable conformational states, an automated clustering algorithm within *UCSF Chimera* was implemented.[47] The theoretical analysis revealed 56 distinct conformational states for WT, and 80 states for M2. Representative structures from the top three most frequent conformational states are shown in Fig. 5a, along with a composite structure of the three states superimposed. For WT, states 1, 2, and 3 composed 35%, 15% and 8% of the 200 ns simulation, respectively. For M2, states 1, 2, and 3 composed 27%, 13%, and 9% of the simulation time, respectively. All other observed conformational states for WT and M2 compose the remaining 42% and 51% of their respective simulations. Individually, these infrequent states each lasted for less than 7% of the simulation. Additional discussion on ensemble clustering and structural transitions can be found in the supplementary.

As evidenced by the representative structures in Fig. 5a, amino acids Val-Thr-Glu-Ser form an α-helical structure in both peptides. Based on the residence time, the α-helix is more stable in WT than M2. Composite structures of states 1, 2, and 3 for WT, Fig. 5a, shows the overall conformation is (i) quite similar regarding the high structural overlap for the α-helix, and, (ii) different in the relative location of the tyrosine rings. For M2, states 1 through 3 show little structural overlap since (i) state 1 lacks the α-helix present in the other states, and (ii) the α-helices in state 2 and 3 do not align as observed with WT. Thus, WT is more uniformly structured in solution than M2. Inspection of amino-acid contacts revealed that Trp12 in M2 made frequent contacts with the N-terminal amino acids potentially destabilizing the observed secondary structure (Supplementary Fig. 7). These side-chain contacts were much less frequent with

Tyr12 in WT providing a rationale for why the substitution of Trp affects the molecular structure of the peptide. This suggests that truncating the peptide to remove Trp12 may stabilize the structure.

Additional structural comparisons between WT and M2 are provided in greater detail in the supplementary. Backbone angle population distributions of WT and M2 were similar, however M2 sampled more conformational space suggesting greater conformational entropy (Supplementary Fig. 4). From said angle distributions, backbone entropies for WT and M2 were estimated as 563 and 597 J/mol K, respectively. Using the relationship between frequency/probability and energetics, we estimated the free energy values for all the observed conformational states. For states 1, 2 and 3, *i.e.*, the lowest energy states, we estimated free energies of 1.56, 4.36, and 6.23 kJ/mol, respectively, for WT, and energies of 2.47, 4.82, and 5.81 kJ/mol for M2 (Fig. 5a). All other observed conformational states for WT and M2 were determined to be high energy states given their low frequency. It is important to note that for WT, the free energy differences between state 1 and the other states exceeds the molar thermal energy, *RT*, at room temperature, while the energy differences between all M2 conformational states is less than the molar thermal energy. This goes along with the suggestion that M2 is more structurally disperse in solution than WT at room temperature.

To estimate the structural dispersity differences between solvated WT and M2, we determined the probability of every observed conformational state using Boltzmann statistics (Fig. 5b). At room temperature, the lowest energy WT state, state 1, is the most probable conformation (44%), outnumbering the collection of all the high energy infrequent states. For M2, the
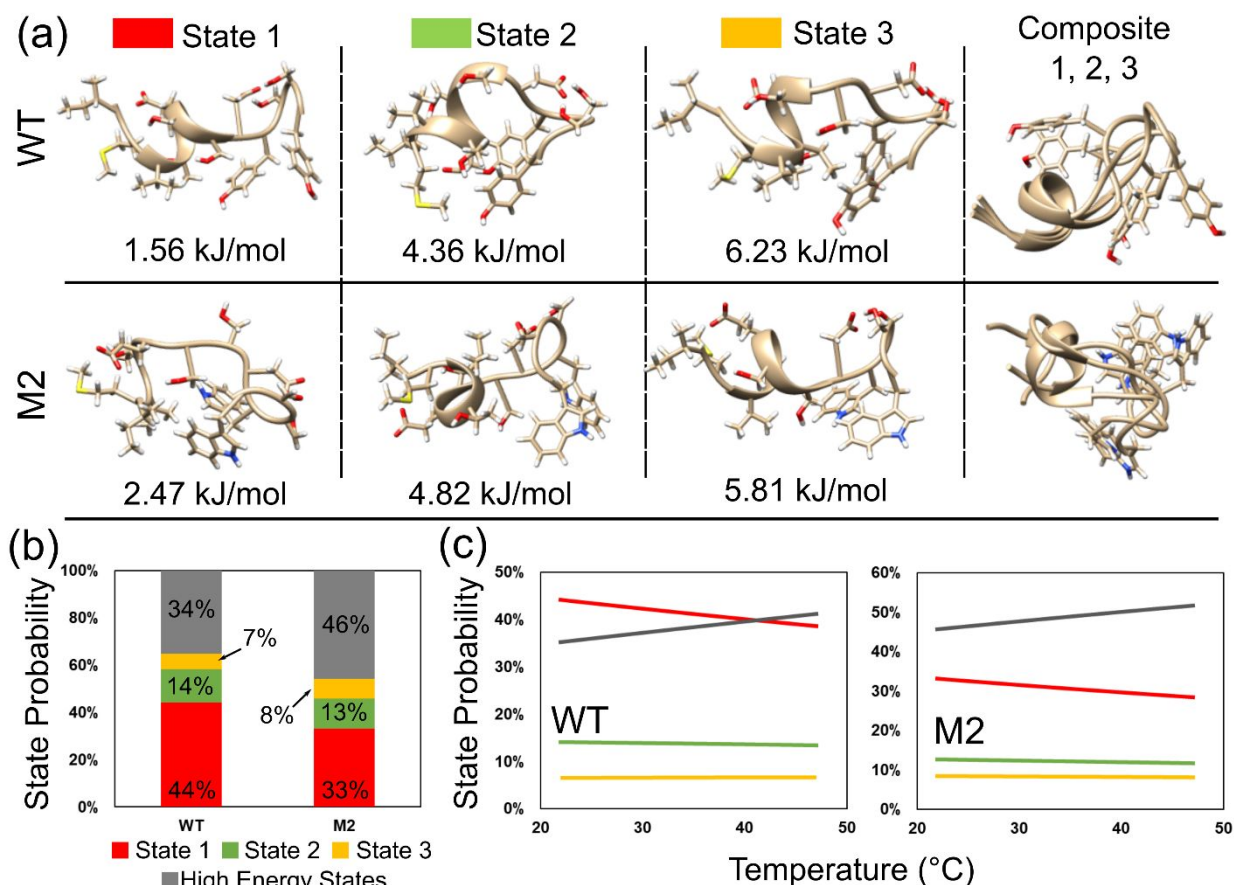
ARTICLE

Fig. 5 Conformational Propensities and Energetics of Solvated GrBP5s. (a) Representative structures of the three most stable states as determined by proportion of simulation time and ensemble clustering. The inset energetic values are based on the probability of the peptide being in the given conformational state out of all the observed states during the 200 ns simulation using $G = -RT \times ln[p_i/(1-p_i)]$ in which p_i is the probability of the state. The comparison of the three states was obtained by aligning the peptide by amino acid sequence and orienting to obtain the lowest Cα RMSD value. (b) The room-temperature structural dispersity of the solution state was estimated using a Boltzmann distribution, and the free energy estimates based on conformational state probabilities. The high energy states are the collection of infrequent states observed for the respective peptide (n= 53 for WT and n=77 for M2). (c) The temperature dependence of the solution dispersity for WT and M2 was then estimated using the same Boltzmann distribution.

collection of high energy infrequent states is the most dominant (46%). If we assume that the adsorption rates of the various conformational states are on the same order of magnitude, then we can assume that the surface adsorbed M2 is similarly disperse to the solution state. This finding supplements our experimental results by elucidating the non-uniformity of solute conformation as cause for M2 forming an amorphous rather than ordered room-temperature assembly. Assembly of a more conformationally uniform peptide in solution, like WT, is not impeded by an additional kinetic conformational transition.

Estimation of the solution dispersity as a function of temperature shows that at approximately 40 °C the collection of high energy WT states, *i.e.*, all states besides states 1, 2 and 3, overcome state 1 to be the most probable in solution (Fig. 5c). This finding further suggests denaturation as the mechanism leading to the experimentally observed decrease in adsorption and degree of ordering. For M2, the collection of high energy states remains the most probable with increasing thermal energy. The experimentally observed increase in ordering for M2 then can be interpreted as a result of populating an infrequent state with greater propensity to assemble. State 3 of M2 is one such conformational state given it is within 0.6 Å RMSD of WT's state 1. However, the population

increase of M2's state 3 is minimal compared to the increase in the high energy states (Fig. 5c). Since our analysis relies on conformational states observed at 298K, the sampling of high energy states of interest is limited, *i.e.*, the conformational state of interest could not have been observed in our simulations.

The presented computational results supplement our experimental analysis of WT and M2 on HOPG and broaden our understanding of polypeptide assembly and thermal effects prior and post assembly. Taking the experimental and computational results collectively an assembly mechanism for graphite-binding peptides can be developed. As schematized in Fig. 6, ordered assembly results when the solution state has a large population of a conformation with propensity for assembly, allowing it to adsorb, diffuse, and interact with other peptides to form a long range ordered structure. In the case of M2, thermal energy aids in the transition to this assembly prone conformation both in solution and at the surface. Amorphous assembly results when a more conformationally disperse peptide adsorbs, retains the dispersity and simply aggregates upon interacting with other peptides.
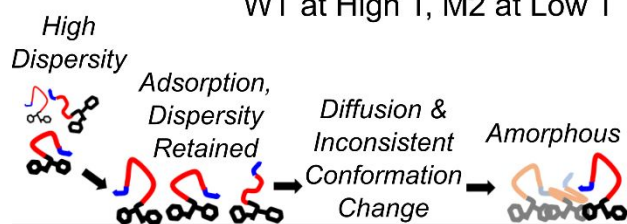
Conclusions
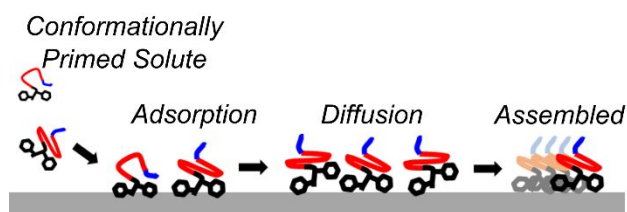
Fig. 6 Proposed mechanism for thermally directed and conformationally mediated self-assembly of graphite-binding peptides. For simplicity the scheme only shows the WT structure. The blue, red and black colouring represents the hydrophobic, hydrophilic and aromatic domains of the peptide respectively.

In this complementary experimental and computational study of peptide conformational dynamics, adsorption kinetics and structural characterization of the assembled state, it is shown that the self-assembly of "soft" (conformationally flexible) biomolecules, can be directed by specific environmental conditions that affect the structural dispersity of the solvated molecules. Peptides with structurally uniform solution conformations, for example WT, readily self-organize into long-range ordered nanostructures, given the peptide conformation has a propensity to assemble. Increasing the thermal energy elevates the dispersity of the peptide conformations in solution, which negatively impacts the adsorption and assembly process. Similar to the case of thermal destabilization, peptides that are already conformationally disperse at room-temperature, such as M2, do not readily assemble. Interestingly, increasing the supplied thermal energy allows peptides, such as M2, to sample the conformational space, and consolidate to a structure with increased propensity for self-assembly.

The profound effect of temperature on the adsorption kinetics and assembly behavior of these two solid-binding peptides suggests that SBPs are conformationally tunable, and thus, belong to the class of stimuli responsive materials that have use for a wide variety of practical applications, such as functional bioelectronic devices. From a general fundamental perspective these results expand the view of the effect of temperature on the molecular assembly process. For conformationally "soft" molecules, the temperature does not only affect the assembly kinetics, but also changes the aggregation structure due to the modification of solution conformational states.

Our on-going research includes computational modeling of peptide conformational dynamics and energetics at elevated temperatures to further validate the proposed assembly mechanism. To fully understand the effects of temperature on the self-assembly process, knowledge of both the solvated and surface adsorbed peptide conformations at lower and elevated temperatures will be required. Additionally, on-going research included the experimental interrogation of the key intermolecular interactions present in the peptide assemblies.

## Conflicts of interest

There are no conflicts to declare.

Acknowledgements

References

1.   L. P. Kozlowski, *Biology direct*, 2016, **11**, 55.
2.   G. M. Whitesides and B. Grzybowski, *Science*, 2002, **295**, 2418-2421.
3.   D. Philp and J. F. Stoddart, *Angewandte Chemie International Edition in English*, 1996, **35**, 1154-1196.
4.   M. Zerial and H. McBride, *Nature reviews Molecular cell biology*, 2001, **2**, 107.
5.   A. Mallavarapu and T. Mitchison, *The Journal of cell biology*, 1999, **146**, 1097-1106.
6.   S. Zhang, *Nature biotechnology*, 2003, **21**, 1171.
7.   Y. Lin, A. Böker, J. He, K. Sill, H. Xiang, C. Abetz, X. Li, J. Wang, T. Emrick and S. Long, *Nature*, 2005, **434**, 55.
8.   J. C. Love, L. A. Estroff, J. K. Kriebel, R. G. Nuzzo and G. M. Whitesides, *Chemical Reviews*, 2005, **105**, 1103-1170.
9.   T. Kato, *Science*, 2002, **295**, 2414-2418.
10. L. Zang, Y. Che and J. S. Moore, *Accounts of chemical research*, 2008, **41**, 1596-1608.
11. F. Li, D. P. Josephson and A. Stein, *Angewandte Chemie International Edition*, 2011, **50**, 360-388.
12. A. Ulman, *Chemical Reviews*, 1996, **96**, 1533-1554.
13. J. N. Israelachvili, D. J. Mitchell and B. W. Ninham, *Journal of the Chemical Society, Faraday Transactions 2: Molecular and Chemical Physics*, 1976, **72**, 1525-1568.
14. A. Ciesielski, C. A. Palma, M. Bonini and P. Samorì, *Advanced Materials*, 2010, **22**, 3506-3520.
15. D. K. Schwartz, *Annual Review of Physical Chemistry*, 2001, **52**, 107-137.
16. D. E. Koshland Jr, *Angewandte Chemie International Edition in English*, 1995, **33**, 2375-2378.
17. R. Mannhold, H. Kubinyi and G. Folkers, *Protein-ligand interactions: from molecular recognition to drug design*, John Wiley & Sons, 2006.
18. P. W. Rothemund, *Nature*, 2006, **440**, 297.

ARTICLE

19. S. Gonen, F. DiMaio, T. Gonen and D. Baker, *Science*, 2015, **348**, 1365-1368.

20. A. Aggeli, I. A. Nyrkova, M. Bell, R. Harding, L. Carrick, T. C. McLeish, A. N. Semenov and N. Boden, *Proceedings of the National Academy of Sciences*, 2001, **98**, 11857-11862.

21. J. D. Hartgerink, E. Beniash and S. I. Stupp, *Science*, 2001, **294**, 1684-1688.

22. S. Woo and P. W. Rothemund, *Nature communications*, 2014, **5**, 4889.

23. C. Whitehouse, J. Fang, A. Aggeli, M. Bell, R. Brydson, C. W. Fishwick, J. R. Henderson, C. M. Knobler, R. W. Owens and N. H. Thomson, *Angewandte Chemie International Edition*, 2005, **44**, 1965-1968.

24. E. Györvary, O. Stein, D. Pum and U. Sleytr, *Journal of microscopy*, 2003, **212**, 300-306.

25. J. Israelachvili, *Langmuir*, 1994, **10**, 3774-3781.

26. R. Schulman and E. Winfree, *Proceedings of the National Academy of Sciences*, 2007, **104**, 15236-15241.

27. M. Altman, P. Lee, A. Rich and S. Zhang, *Protein Science*, 2000, **9**, 1095-1105.

28. J. H. Collier, B. H. Hu, J. W. Ruberti, J. Zhang, P. Shum, D. H. Thompson and P. B. Messersmith, *Journal of the American Chemical Society*, 2001, **123**, 9463-9464.

29. A. K. Dunker, J. D. Lawson, C. J. Brown, R. M. Williams, P. Romero, J. S. Oh, C. J. Oldfield, A. M. Campen, C. M. Ratliff and K. W. Hipps, *Journal of molecular graphics and modelling*, 2001, **19**, 26-59.

30. Z. A. Levine, L. Larini, N. E. LaPointe, S. C. Feinstein and J.-E. Shea, *Proceedings of the National Academy of Sciences*, 2015, **112**, 2758-2763.

31. H. J. Dyson and P. E. Wright, *Nature reviews Molecular cell biology*, 2005, **6**, 197.

32. Q. Qiao, G. R. Bowman and X. Huang, *Journal of the American Chemical Society*, 2013, **135**, 16092-16101.

33. M. Sarikaya, C. Tamerler, A. K. Y. Jen, K. Schulten and F. Baneyx, *Nat Mater*, 2003, **2**, 577-585.

34. M. J. Penna, M. Mijajlovic, C. Tamerler and M. J. Biggs, *Soft Matter*, 2015, **11**, 5192-5203.

35. Z. E. Hughes and T. R. Walsh, *Journal of Materials Chemistry B*, 2015, **3**, 3211-3221.

36. C. R. So, Y. Hayamizu, H. Yazici, C. Gresswell, D. Khatayevich, C. Tamerler and M. Sarikaya, *ACS Nano*, 2012, **6**, 1648-1656.

37. C. R. So, J. L. Kulp III, E. E. Oren, H. Zareie, C. Tamerler, J. S. Evans and M. Sarikaya, *Acs Nano*, 2009, **3**, 1525-1531.

38. D. Khatayevich, M. Gungormus, H. Yazici, C. So, S. Cetinel, H. Ma, A. Jen, C. Tamerler and M. Sarikaya, *Acta Biomaterialia*, 2010, **6**, 4634-4641.

39. Y. Hayamizu, C. R. So, S. Dag, T. S. Page, D. Starkebaum and M. Sarikaya, *Scientific reports*, 2016, **6**, 33778.

40. T. Kacar, M. T. Zin, C. So, B. Wilson, H. Ma, N. Gul-Karaguler, A. K. Y. Jen, M. Sarikaya and C. Tamerler, *Biotechnology and Bioengineering*, 2009, **103**, 696-705.

41. M. Hnilova, D. Khatayevich, A. Carlson, E. E. Oren, C. Gresswell, S. Zheng, F. Ohuchi, M. Sarikaya and C. Tamerler, *Journal of colloid and interface science*, 2012, **365**, 97-102.

42. D. Khatayevich, T. Page, C. Gresswell, Y. Hayamizu, W. Grady and M. Sarikaya, *Small*, 2014, **10**, 1505-1513.

43. Z. E. Hughes and T. R. Walsh, *Nanoscale*, 2018, **10**, 302-311.

44. M. Levitt, M. Hirshberg, R. Sharon and V. Daggett, *Computer physics communications*, 1995, **91**, 215-231.

45. D. Beck, D. Alonso and V. Daggett, *Computer Program, University of Washington, Seattle*, 2000.

46. M. Levitt, M. Hirshberg, R. Sharon, K. E. Laidig and V. Daggett, *The Journal of Physical Chemistry B*, 1997, **101**, 5051-5061.

47. E. F. Pettersen, T. D. Goddard, C. C. Huang, G. S. Couch, D. M. Greenblatt, E. C. Meng and T. E. Ferrin, *Journal of computational chemistry*, 2004, **25**, 1605-1612.

48. M. Hnilova, E. E. Oren, U. O. Seker, B. R. Wilson, S. Collino, J. S. Evans, C. Tamerler and M. Sarikaya, *Langmuir*, 2008, **24**, 12440-12445.

49. J. N. Mabry, M. Kastantin and D. K. Schwartz, *ACS nano*, 2015, **9**, 7237-7247.
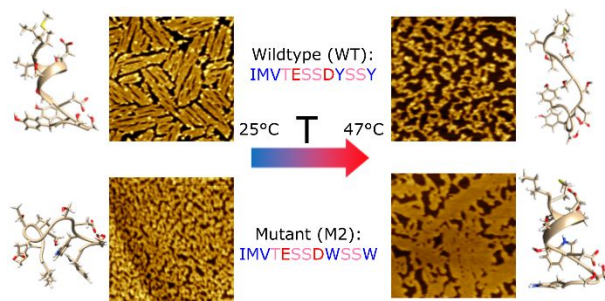
We demonstrate the directed assembly of graphite binding peptides mediated by thermal perturbations to the solvated peptide conformation.